Autosomal Recessive Retinitis Pigmentosa Caused by Mutations in the *MAK* Gene

Edwin M. Stone,[1,2] *Xunda Luo,*[3] *Elise Héon,*[4] *Byron L. Lam,*[5] *Richard G. Weleber,*[6] *Jennifer A. Halder,*[1] *Louisa M. Affatigato,*[1] *Jacqueline B. Goldberg,*[3] *Alexander Sumaroka,*[3] *Sharon B. Schwartz,*[3] *Artur V. Cideciyan,*[3] *and Samuel G. Jacobson*[3]

Purpose. To determine the disease expression in autosomal recessive (ar) retinitis pigmentosa (RP) caused by mutations in the *MAK* (male germ cell-associated kinase) gene.

Methods. Patients with RP and *MAK* gene mutations ($n = 24$; age, 32–77 years at first visit) were studied by ocular examination, perimetry, and optical coherence tomography (OCT).

Results. All but one *MAK* patient were homozygous for an identical truncating mutation in exon 9 and had Ashkenazi Jewish heritage. The carrier frequency of this mutation among 1207 unrelated Ashkenazi control subjects was 1 in 55, making it the most common cause of heritable retinal disease in this population and *MAK*-associated RP the sixth most common Mendelian disease overall in this group. Visual acuities could be normal into the eighth decade of life. Kinetic fields showed early loss in the superior–temporal quadrant. With more advanced disease, superior and midperipheral function was lost, but the nasal field remained. Only a central island was present at late stages. Pigmentary retinopathy was less prominent in the superior nasal quadrant. Rod-mediated vision was abnormal but detectable in the residual field; all patients had rod>cone dysfunction. Photoreceptor layer thickness was normal centrally but decreased with eccentricity. At the stages studied, there was no evidence of photoreceptor ciliary elongation.

Conclusions. The patterns of disease expression in the *MAK* form of arRP showed some resemblance to patterns described in autosomal dominant RP, especially the form caused by *RP1* mutations. The similarity in phenotypes is of interest, considering that there is experimental evidence of interaction between Mak and RP1 in the photoreceptor cilium. (*Invest Ophthalmol Vis Sci.* 2011;52:9665–9673) DOI:10.1167/iovs.11-8527

A homozygous Alu insertion in exon 9 of the *MAK* (male germ cell–associated kinase) gene was recently identified as the cause of disease in an isolated patient with retinitis pigmentosa (RP). Twenty additional probands were then found to be homozygous for this insertion.[1] Another recent study involving other populations identified a further eight patients with RP and other *MAK* mutations.[2] *MAK* encodes a kinase involved in the regulation of photoreceptor connecting cilium length.[3] In human retina, MAK is expressed in the inner segments, cell bodies, and axons of rod and cone photoreceptors.[1]

We asked whether genotype was the only distinguishing feature of this type of autosomal recessive (ar) RP, of which there are many other molecular forms.[4,5] Noninvasive techniques were used to study the phenotype of patients with *MAK* mutations; many of the patients had been followed for years to decades. There was a specific visual field pattern in early stages and longitudinal data provided a preliminary view of the natural history of rod and cone visual loss. All but one of the patients had Ashkenazi Jewish (AJ) heritage, an association caused by specific mutations in *CLRN1*,[6] *PCDH15*,[7] and *DHDDS*[8,9] that has also been observed in RP.

The phenotypic features that we noted in RP patients with *MAK* mutations may permit a more directed gene search in simplex or multiplex RP patients and lead to identification of an increased number of arRP patients with this molecular diagnosis. An available murine model, the *Mak*-knockout mouse,[3] enhances the opportunity to perform proof-of-concept research and make progress toward human therapy.

Methods

Human Subjects

Twenty-four patients representing 22 families (Table 1) with the clinical diagnosis of RP and disease-causing mutations in the *MAK* gene were studied. Patients had a complete eye examination, including electroretinograms (ERGs) in most cases. Informed consent was obtained. Procedures followed the Declaration of Helsinki and had institutional review board approvals.

Molecular Analyses

A 353-base-pair insertion in MAK exon 9 was identified in patient 14 by using a combination of next-generation and Sanger sequencing, as described elsewhere.[1] Single-strand conformational polymorphism

From the [1]Department of Ophthalmology and Visual Sciences and the [2]Howard Hughes Medical Institute, University of Iowa Carver College of Medicine, Iowa City, Iowa; the [3]Scheie Eye Institute, Department of Ophthalmology, University of Pennsylvania, Philadelphia, Pennsylvania; the [4]Department of Ophthalmology and Vision Sciences, Hospital for Sick Children, University of Toronto, Toronto, Ontario, Canada; the [5]Bascom Palmer Eye Institute, University of Miami Miller School of Medicine, Miami, Florida; and the [6]Oregon Retinal Degeneration Center, Casey Eye Institute, Oregon Health and Science University, Portland, Oregon.

Supported by grants from the Howard Hughes Medical Institute, National Eye Institute (R01EY016822), the Grousbeck Family Foundation, the National Neurovision Research Institute, the Foundation Fighting Blindness, Hope for Vision, and the Macula Vision Research Foundation. AVC is a Research to Prevent Blindness Senior Scientific Investigator.

Submitted for publication September 2, 2011; revised October 24, 2011; accepted November 10, 2011.

Disclosure: **E.M. Stone**, None; **X. Luo**, None; **E. Héon**, None; **B.L. Lam**, None; **R.G. Weleber**, None; **J.A. Halder**, None; **L.M. Affatigato**, None; **J.B. Goldberg**, None; **A. Sumaroka**, None; **S.B. Schwartz**, None; **A.V. Cideciyan**, None; **S.G. Jacobson**, None

Corresponding author: Edwin M. Stone, The University of Iowa Institute for Vision Research, 375 Newton Road, 4111 MERF, Iowa City, IA 52242; edwin-stone@uiowa.edu.

TABLE 1. Clinical Characteristics of the Patients

Patient	Age at Initial Visit (y)/Sex	Eye	Visual Acuity*	Refraction	Multiple Visits†	Kinetic Visual Field Extent (V-4e/I-4e)‡	ERG§	
							Rod b-Wave	Cone Flicker
P1	32/M	RE	20/20	−5.00	X	87/42	ND	↓ ↓
		LE	20/20	−5.00				
P2	37/M	RE	20/20	−4.25 −2.50 × 180	X	4/<1	NP	NP
		LE	20/30	−3.75 −2.00 × 135				
P3	37/M	RE	20/30	−6.00	X	72/11	ND	↓ ↓
		LE	20/20	−5.50				
P4‖	39/M	RE	20/20	−3.75 −1.50 × 009	X	67/22	NP	NP
		LE	20/20	Pseudophakia				
P5	40/M	RE	20/25	−6.75 −2.75 × 030	X	92/9	NP	NP
		LE	20/20	−4.50 −2.75 × 160				
P6	41/M	RE	20/60	−6.00		15/<1	ND	↓ ↓ ↓
		LE	20/30	−4.25				
P7	43/M	RE	20/20	−0.25 −0.75 × 055	X	NA	ND	↓ ↓ ↓
		LE	20/20	−0.75 −0.25 × 055				
P8	44/M	RE	20/20	+1.00 −2.00 × 060	X	100/42	ND	↓
		LE	20/30	+1.50 −1.50 × 010				
P9	48/M	RE	20/20	+0.25 −1.00 × 110	X	39/13	↓ ↓	↓
		LE	20/20	+0.50 −1.00 × 090				
P10	48/M	RE	20/30¶	+0.50 −0.75 × 087¶	X	10/2#	↓ ↓¶	↓ ↓¶
		LE	20/20¶	+0.25 −0.50 × 090¶				
P11	54/M	RE	20/25	+1.50 −1.25 × 010	X	24/4	ND	↓ ↓ ↓
		LE	20/20	+1.50 −2.00 × 170				
P12‖	56/F	RE	20/30	−4.75 −0.75 × 110	X	2/<1	ND	ND
		LE	20/40	−5.00				
P13‖	56/M	RE	20/25	Plano		66/30	NP	NP
		LE	20/20	Plano				
P14	58/M	RE	20/25	Plano −0.50 × 150		<1/<1	NP	NP
		LE	20/30	+1.00 −1.00 × 130				
P15	59/F	RE	20/50	+3.00 −1.50 × 020	X	<1/<1	ND	ND
		LE	20/60	+3.75 −1.50 × 002				
P16‖	65/F	RE	20/20	Plano−1.00 × 090	X	76/8	ND	↓ ↓ ↓
		LE	20/40	Plano −1.00 × 090				
P17	67/F	RE	20/20	−1.00		NA	↓ ↓	↓ ↓
		LE	20/20	−1.00				
P18	69/F	RE	20/50	+1.50 −0.75 × 015	X	7/3	ND	ND
		LE	20/40	+1.00 −0.50 × 180				
P19	69/M	RE	20/40	+1.00 −1.00 × 030	X	4/<1	ND	↓ ↓ ↓ ↓
		LE	20/20	+0.50				
P20	69/M	RE	20/50	+0.50		77/34	↓ ↓ ↓	↓
		LE	20/60	+0.50				
P21	70/F	RE	20/30	Pseudophakia		<1/<1	ND	ND
		LE	20/30	Pseudophakia				
P22	71/F	RE	20/200	−3.75	X	<1/<1	ND	ND
		LE	3/200	NP				
P23**	76/M	RE	HM	Pseudophakia		NA	ND	ND
		LE	HM	−1.00				
P24	77/M	RE	20/30	NP		46/1	ND	↓
		LE	20/20	Pseudophakia				

NP, not performed; ND, not detectable; NA, not available.

* Best corrected visual acuity.

† Two or more visits.

‡ Average of eyes; expressed as a percentage of normal mean of responses to the V-4e or I-4e target; 2 SD below normal equals 90% (Jacobson et al.[10]); average both eyes.

§ Detectable ERGs are described qualitatively: ↓, moderately reduced; ↓ ↓, markedly reduced; ↓ ↓ ↓, barely detectable.

‖ P4 and P13 are siblings; P12 and P16 are third cousins.

¶ At age 48.

At age 50.

** *MAK* genotype: Asn130His/Lys22Asn. All other patients were homozygous for the 353-base-pair insertion in exon 9.

analysis (SSCP) was then used to screen a cohort of 1798 probands affected with autosomal recessive or simplex RP were then screened for the presence of this insertion, as described.[1] Two hundred unrelated RP probands and two hundred normal controls were screened for mutations in the entire coding sequence of *MAK*, using next-generation sequencing of pooled DNA samples. To establish the AJ carrier frequency of the *MAK* exon 9 insertion and the Lys42Glu variation in *DHDDS*, DNA samples from 1207 unrelated, anonymous AJ individuals were obtained from Dor Yeshorim (New York, NY), and SSCP was used to screen for these two variations. All positive SSCP results and all putative disease-causing variations observed during the next-generation sequencing experiment were confirmed with automated bidirectional Sanger sequencing (model 3730; Applied Biosystems [ABI], Foster City, CA).

Visual Function and Retinal Structure

Perimetry. Kinetic perimetry was performed and visual field extent was analyzed as previously reported.[10] Static thresholds were determined with stimuli (1.7° diameter, 200 ms duration) under dark-adapted (500 and 650-nm stimuli) and light-adapted (600 nm) conditions. A full-field test of 71 loci on a 12° grid and a horizontal profile across the fovea (extending 60° at 2° intervals) were used. Photoreceptor mediation was determined by the sensitivity difference between detection of 500- and 650-nm stimuli.[11,12] Rod (500 nm, dark-adapted) and cone (600 nm, light adapted) sensitivity losses at each test locus were calculated by comparison with normal mean sensitivities at the location. Loci were considered to have no measurable rod sensitivity if loss was >30 dB.[12]

Optical Coherence Tomography. Retinal cross sections were obtained with OCT in *MAK* RP patients ($n = 7$; age, 51–80 years at time of OCT), RP patients without *MAK* mutations ($n = 11$; age, 22–65), and normal subjects ($n = 26$; age, 8–66). Data collection used three instruments: a time-domain (TD) system (OCT3; Carl Zeiss Meditec, Dublin, CA) and two spectral-domain (SD) systems (RTVue-100; Optovue Inc., Fremont, CA; and Spectralis, Heidelberg Engineering, Vista, CA). Postacquisition processing of OCT data were performed with custom programs (MatLab 6.5; The MathWorks, Natick, MA). Recording and analysis techniques are published.[13–16] In brief, OCTs were performed along the vertical meridian from the fovea into superior and inferior retinas. Longitudinal reflectivity profiles (LRPs) making up the OCT scans were aligned by straightening the major RPE reflection. Retinal thickness was measured from the vitreoretinal interface to the RPE signal.[17] The outer photoreceptor nuclear layer (ONL) was defined in regions of scans showing two parallel stereotypical hyporeflective layers between the RPE and vitreoretinal interface. Inner retinal thickness was defined as the distance between the signal transition at the vitreoretinal interface and the sclerad boundary of the inner nuclear layer (INL) or the single hyporeflective layer continuous with the INL. Normal data for total retinal thickness, ONL, and inner retinal thickness obtained with the TD-OCT have been published.[15–17] The thickness of the inner and outer segments (IS+OS) was measured by using SD-OCT data from the ONL to the RPE layer at the foveal depression (for a cone estimate) and at 2, 3, and 4 mm superior to the fovea in the vertical meridian (rod-dominated estimates). ONL and IS+OS parameters measured in *MAK* RP were compared with RP patients without *MAK* mutations and a subset of the normal subjects ($n = 10$; ages 8–45 years).

Results

Molecular Findings

A combination of next-generation exome sequencing and conventional Sanger sequencing identified a homozygous 353-base-pair insertion in exon 9 of the *MAK* gene in patient (P)14 of this cohort[1] (Table 1). SSCP was then used to screen 1798 unrelated probands with autosomal recessive or simplex RP, and 20 additional individuals were found to be homozygous for the same exon 9 insertion. Two of these 20 individuals had an affected relative who was also found to be homozygous for this mutation. These 23 individuals all had known Jewish ancestry, and their clinical findings are summarized in Table 1.

Next-generation sequencing of *MAK* coding sequences amplified from a pool of 200 RP patients and another pool of 200 control individuals revealed only a single plausible disease-causing variant (Asn130His) in an individual with simplex RP. This variant was previously identified by Ozgul et al.[2] workers in one member of their cohort of *MAK*-associated RP patients. Sanger sequencing of the complete *MAK* coding sequence of this individual revealed a second plausible disease-causing variant (Lys22Asn) that has not been reported. Analysis of this individual's children revealed that these two *MAK* variants lie on separate alleles. When first evaluated, this compound heterozygous individual (P23, Table 1) was 76 years of age and had hand-motions vision, a nondetectable ERG, and extensive pigmentary change in all four quadrants of the retina.

We next investigated the carrier frequency of the *MAK* exon 9 insertion among 1207 unrelated individuals of AJ ancestry. We found 22 individuals in this cohort (1/55) to be heterozygous for this variant. Thus, approximately 1 in 12,000 individuals with two AJ parents would be expected to have *MAK*-associated RP caused by homozygosity of this mutation. If this population is affected with RP at a rate that is similar to that in the general population (i.e., 1 in 4000), the homozygosity of the exon 9 insertion in *MAK* would cause about one third of all RP in this population. A second RP-causing founder mutation was recently identified among individuals of AJ ancestry, Lys42Glu in *DHDDS*.[8,9] To determine the relative impact of these two RP-causing mutations among the Ashkenazi population, we also screened 1207 AJ control samples for the Lys42Glu variant and identified 10 heterozygotes (1/120). Thus, approximately 1 in 58,000 individuals of AJ ancestry would be expected to have *DHDDS*-associated RP caused by homozygosity of this mutation.

Comparison of these carrier frequencies with those of the 16 most common heritable diseases among AJ individuals[18] has shown that *MAK*-associated RP is the most common eye disease (4.8 times more common than RP caused by mutations in *DHDDS* and *CLRN1*) and the sixth most common Mendelian disease overall in the AJ population.

Clinical Characteristics of the Patients

In this cohort of 24 patients with *MAK* mutations, all but one (P23) was of AJ ancestry and was homozygous for the 353-base-pair insertion in exon 9. The clinical features of the 24 individuals are summarized in Table 1. Among the 23 patients with AJ ancestry and the homozygous exon 9 insertion, visual acuity was 20/50 or better in at least one eye (exception being P22, age 71). All available data (at first visit and in follow-up) showed that 9 of 23 patients retained this acuity into the seventh decade of life and 5 of 23 into the eighth decade. Refractive errors (spherical equivalent; both eyes averaged) of the patients in the present study ranged from −7.00 to +1.00 (mean ± SD, −1.83 ± 2.82; $n = 21$ patients). ERGs were performed in 18 of 23 patients. Five patients showed no detectable ERG waveforms; the remaining 13 patients all had detectable cone flicker, but only 4 had detectable rod ERG b-waves.

All patients were noted to have typical features of RP such as pigmentary changes in the midperipheral retina, vessel attenuation, and waxy pallor of the optic nerve head. Fundus photographs were not routinely taken in the patients in this study. It is of interest, however, that photographs available for two patients (P4 and P8) showed less pronounced pigmentary abnormalities in the superior temporal retinal quadrant outside the vessel arcades (Fig. 1). Kinetic perimetry at different ages in these two patients indicated more preserved function in the inferior nasal visual field, thereby relating to the distribution of funduscopic abnormalities.

Patterns of Visual Loss by Kinetic Perimetry

Kinetic perimetry results showed different patterns of visual field abnormalities among the patients with *MAK* mutations. The cross-sectional data and some longitudinal data from patients over years to decades suggested a disease sequence. Patterns of increasing visual loss, numbered from I to V, were used to organize the perimetry results (Fig. 2A). Pattern I shows a nearly full extent of field with the V-4e target and absolute scotomas, if any, are in the superotemporal quadrant

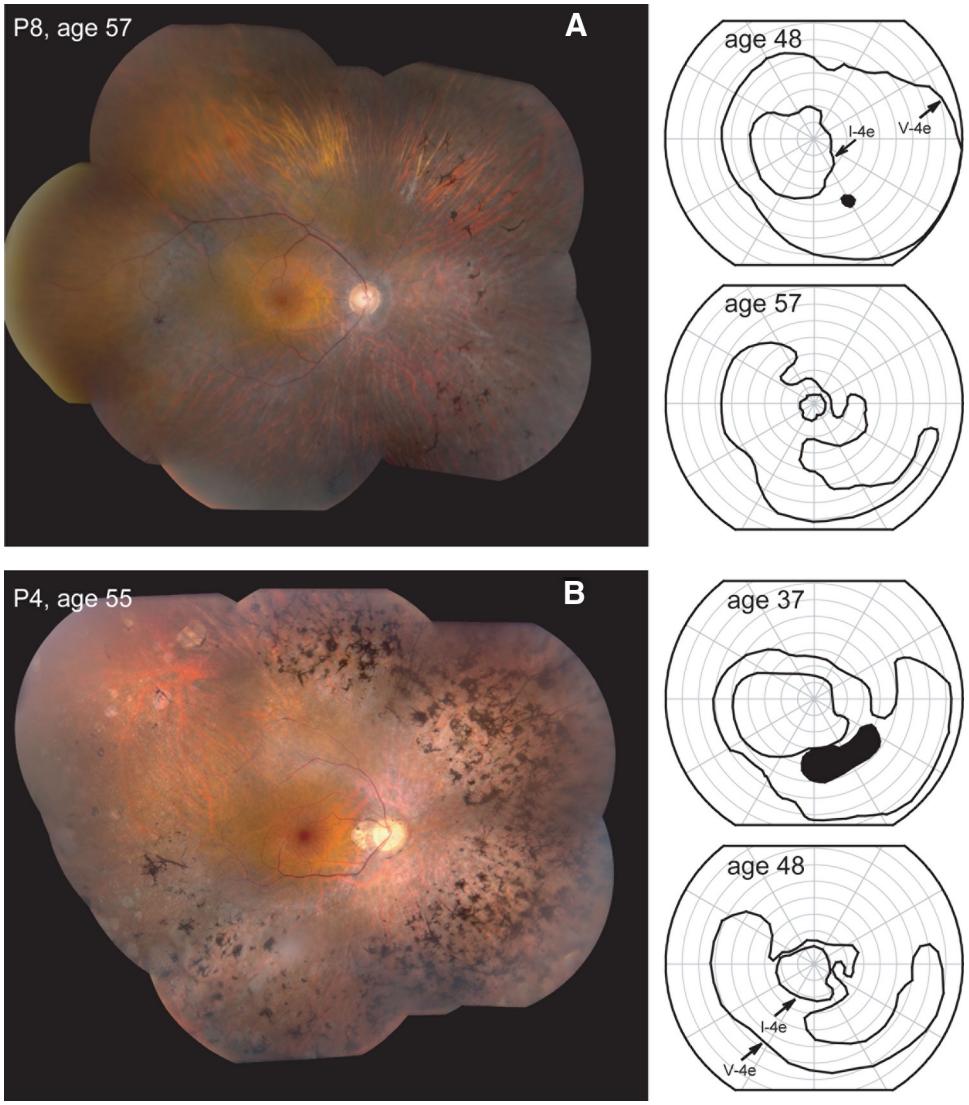

FIGURE 1. Funduscopic abnormalities and corresponding kinetic perimetry results in two patients with *MAK* mutations. **(A)** *Left*: P8, age 57, showed typical fundus findings of RP; the sparse pigmentary abnormalities and thinned-appearing RPE (with visible choroidal vessels) were mainly in the nasal retina. *Right*: kinetic fields (V-4e and I-4e targets) at two ages for P8. At both ages, there was more preserved nasal field function. **(B)** *Left*: P4, age 55, showed dense pigmentary changes in three quadrants but relative sparing of the superotemporal quadrant, even though there were patches of chorioretinal atrophy therein. *Right*: kinetic perimetry of P4 at two younger ages, showing greater nasal than temporal field preservation.

(P16, P5). Patients with *MAK* mutations could also retain substantial visual field with the smaller I-4e target, which could extend from the central field into the inferior nasal quadrant (e.g., P1, Fig. 2A; P8 and P4, Fig. 1). Pattern II was characterized by a large absolute scotoma in the superotemporal field with extension into the inferotemporal midperipheral field. The nasal field was relatively intact. Visual field extent with the I-4e target was limited mainly to the central field. Pattern III showed preservation of much of the nasal field but the temporal field was almost completely undetectable when the V-4e target was used. Preservation of a central island and possibly a nasal field island occurred with the I-4e target (P11). In pattern IV, there was isolation of the central island from islands of residual nasal field by a complete midperipheral scotoma. Pattern V was only a residual small central island of function with V-4e and an even smaller island with I-4e. Longitudinal data through at least three of the patterns were available for P16 (I-III); and two of the patterns for P1 (I and V), P5 (I and II), and P11 (III and IV).

Kinetic field data for all patients, all visits and both target sizes are plotted as a function of age (Fig. 2B). Qualitative observation suggests similarities between patients in the rate of decline of function but differences in the age of onset of these declines. To determine the progression of visual field loss in patients with *MAK* mutations, we used a subset of patients with available longitudinal data (six patients, intervals of 6–13 years; median = 9 years) and assumed a model wherein the disease progresses exponentially after its onset.[6,19–22] Exclusions from this longitudinal analysis were P1, who had only two data points 20 years apart, and P2, who had only a small central island from the first visit. The reliability of exponential curve fitting was affected under both circumstances. Estimated rates of visual field loss were 11% per year for the large target and 18.4% per year for the small target.[23,24] Replotting of the longitudinal visual field data as a function of time after the age of onset showed a substantially reduced scatter (Fig. 2B, right). An invariant exponential rate of progression was assumed and individual ages of disease onset (estimated from the intercepts) ranged from 30 to 63 years (from 30 to 55 for I-4e and from 39 to 63 for V-4e).

Rod and Cone Vision in RP due to *MAK* Mutations

Rod- and cone-mediated sensitivity and the regional variation of each were measured across the visual field in a subset of patients with *MAK* mutations and displayed as maps of sensitivity loss (Fig. 3A). In milder disease, represented by P20 at age 69, there are superotemporal field rod scotomas and relative preservation of inferior and inferonasal loci (corresponding to the superior and superotemporal retina). A similar map

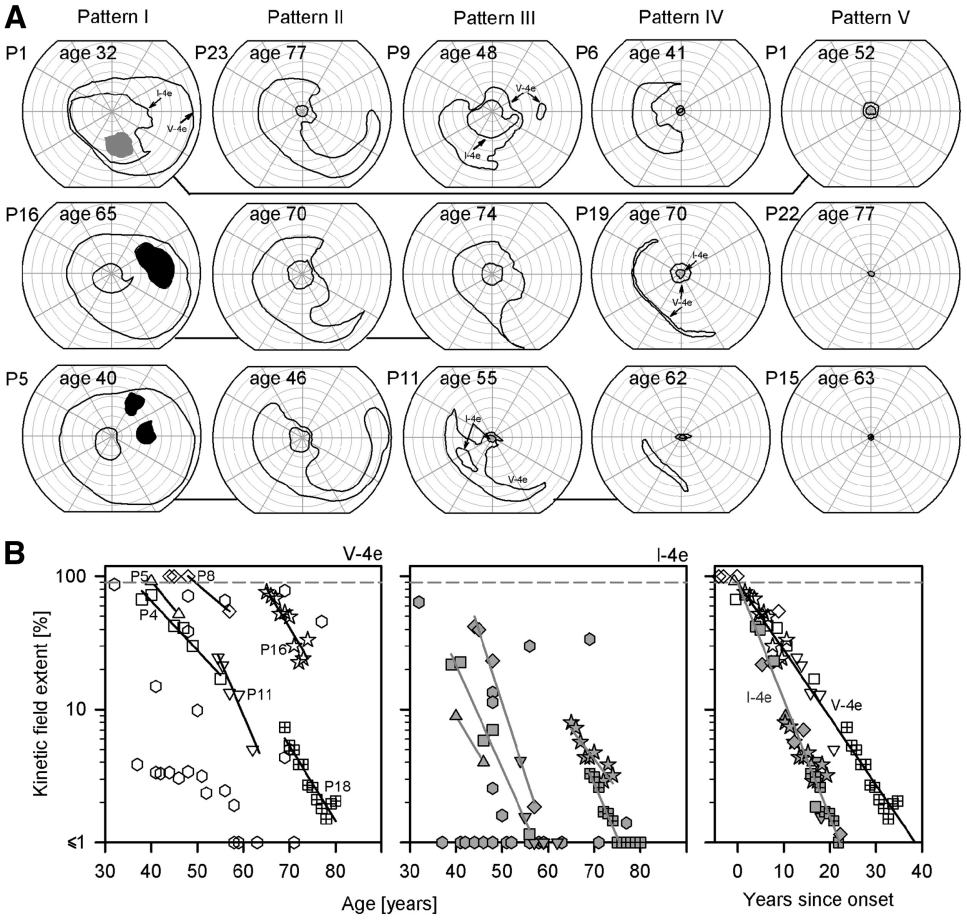

FIGURE 2. Patterns of visual function by kinetic perimetry. (**A**) Kinetic visual field maps showing responses to the V- and I-4e targets. Fields are organized into patterns numbered I–V, with each column representing a different pattern. Patient numbers (Table 1) are at the *top left* of each map. Longitudinal data for patients are shown on the same row, and the maps are connected by lines near the base of the fields. When unmarked, isopters for the I-4e target are interior to the V-4e isopters. *Black areas*: absolute scotomas; *gray areas*: relative scotomas. All fields are depicted as right eyes. (**B**) *Left*: Visual field extent expressed as a percentage of normal mean for the V-4e stimulus and plotted as a function of age. Patient numbers are marked close to the symbols representing their data in the plot. *Solid lines*: fits to data from patients with multiple visits; *hexagons*: data from all other patients not used for fitting; and *dashed line*: 2 SD below normal mean field extent.[10] *Middle*: I-4e extent depicted in the same format as for the V-4e data. Symbols and lines are gray. *Right*: longitudinal data corrected for a variable age of disease onset; kinetic field constriction for the I-4e stimulus shows a faster progression rate compared with that of the V-4e stimulus.

is present for cone sensitivity loss. P1 at age 32 had rod dysfunction across most of the temporal mid- and far-peripheral visual field. At this stage of rod disease in P1, there was less cone dysfunction, with some detectable temporal peripheral function, but this tended to be more reduced in sensitivity than was the central and nasal field function. In more severe disease, represented by P11 at age 55, there was no detectable rod function in three of four quadrants and only a patch of dysfunctional rods inferonasally and in a central island. The cone sensitivity loss map mirrors the findings for rod sensitivity loss with preserved inferonasal and central islands only.

Central cone function assessed with best corrected visual acuity varied between 20/20 (logMAR 0.0) and 20/60 (logMAR 0.48) for most of the patients' lives (Fig. 3B). Rod- and cone-mediated vision was also studied across the central 60° of field (Fig. 3B). Longitudinal data in three patients reveal patterns of progression. As data from P1 at age 32 indicate, rod sensitivity could be within normal limits for almost a 30° expanse of central field; cone-mediated vision also was normal across this expanse but extended to even further eccentricities. A 20-year interval between visits by P1 shows that there was only a central island remaining at age 52 and rod function had become reduced by at least 2 log units (Fig. 2A, pattern V); by light-adapted testing, the central cone island also had abnormally reduced sensitivity. P2 and P11 had central visual data that are probably representative of changes that could have occurred between the extremes in vision in P1 at ages 32 and 52. P2 had a central island of reduced rod function at age 45, and this became further reduced at age 51, showing cone mediation at many loci. The two profiles of light-adapted sensitivities overlap, however, indicating little or no change in this 6-year interval. Two data sets in P11, separated by 8 years showed more dysfunction than the data in P2 but less abnormality than in P1 at age 52. A central island with barely measurable rod function and some cone-mediated function at age 54 became more constricted and more cone-mediated at age 62. The light-adapted cone island at these ages did not differ dramatically.

In Vivo Histopathology in *MAK* Mutations

The structure of the retina was assessed with OCT scans along the vertical median crossing the anatomic fovea. Scans in four patients with *MAK* mutations were compared with that of a normal subject; photoreceptor laminae are highlighted (Fig. 4A). The normal retina (45-year-old man) has a foveal depression and the surrounding retina is laminated with low-reflectivity cellular layers and intervening hyperreflective synaptic laminae. P16, at age 74, appeared to have a normal foveal photoreceptor layer thickness but there was decreasing thickness with increasing eccentricity from the fovea. There was a superior–inferior asymmetry with greater extent of the photoreceptor laminae farther into the superior retina than into the inferior retina, implying intraretinal anisotropy of constriction rates with disease progression. The other three patient scans were more symmetrical around the fovea, which appeared to be normal in thickness, but the vertical extent of the photoreceptor laminae was also more reduced.

Total retina, ONL and inner retina in seven RP patients with *MAK* mutations were quantified for thickness across the vertical meridian (Fig. 4B). Data were plotted in relation to normal limits (mean ± 2 SD). Beyond the fovea, the RP retinas became thinned. ONL measurements indicated that the patients could have normal ONL thickness at the fovea but fall below normal

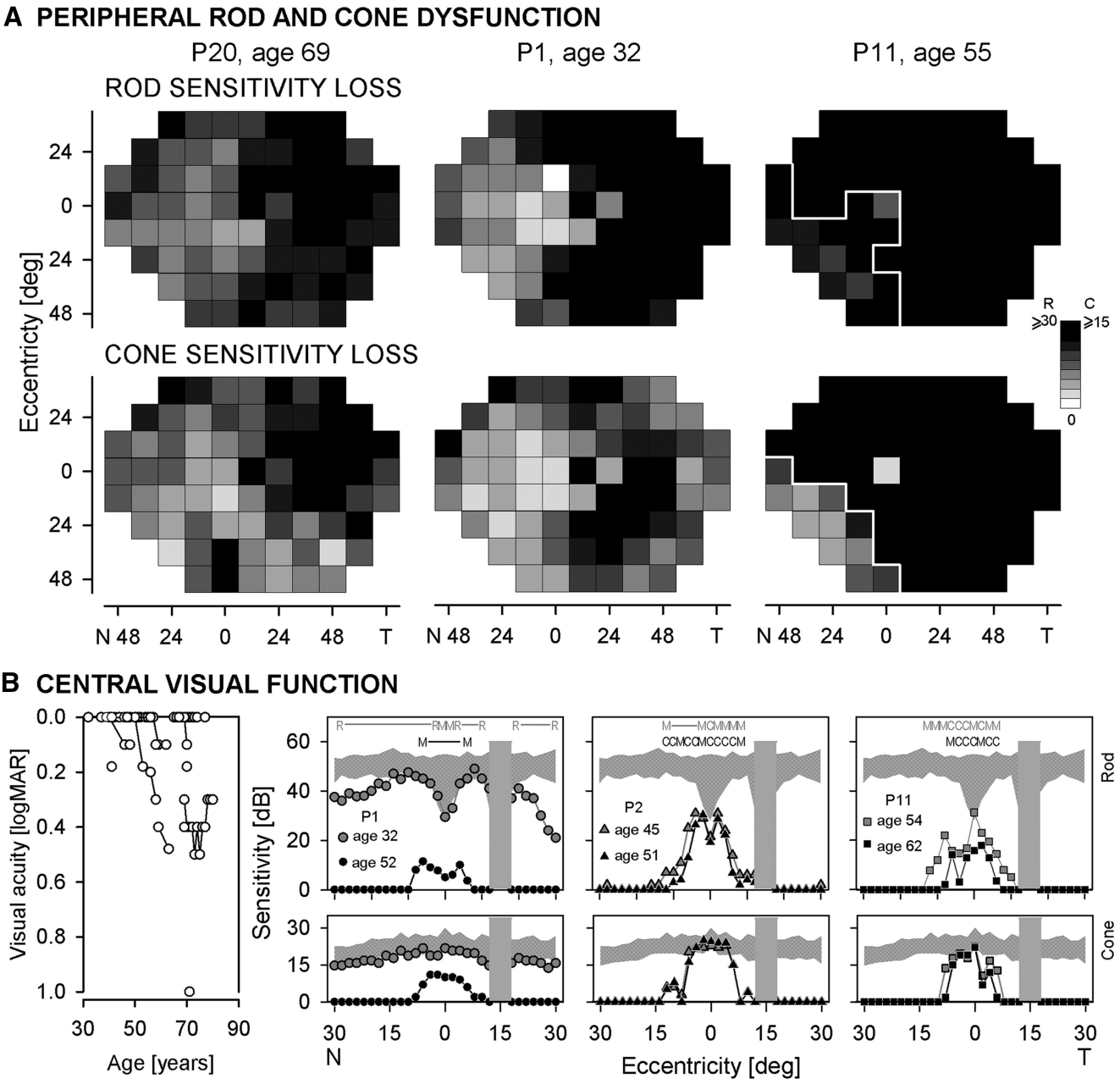

Figure 3. Rod and cone function in RP with *MAK* mutations. (**A**) Topography of rod and cone sensitivity loss across the visual field of three patients representing different severities of disease (*left to right*). *White lines*: outline the boundaries of detectable rod and cone sensitivities in P11. Scale has eight levels of gray representing rod (0 to ≥30 dB) and cone (0 to ≥15 dB) losses; the physiological blind spot is a *black square* at 12° in the temporal field. (**B**) Central visual function assessed by best corrected visual acuity in logMAR as a function of age (*left*; longitudinal data are connected by lines) and (*right*) dark- and light-adapted static perimetric profiles across the horizontal meridian in three patients. Longitudinal data in these three patients demonstrate how central rod (*top*) and cone (*bottom*) visual sensitivity changes with disease progression. R, rod-mediated; M, mixed rod- and cone-mediated; C, cone-mediated; N, nasal; T, temporal visual field. *Dark gray hatched areas*: normal limits (mean ± 2 SD) for rod and cone sensitivities. *Gray bar*, physiological blind spot.

limits in thickness between 2 and 4 mm eccentricity. P9, P16, and P18 showed superior–inferior asymmetry of the ONL. Inner retinal thickness was normally at a minimum in the fovea. At eccentricities beyond ~2 to 3 mm eccentric to the fovea, some patients showed normal inner retinal thickness, whereas others were hypernormal. Such hyperthickness of the paracentral inner retina has been documented in other retinal degenerations and ascribed to retinal remodeling.[6,15,16,25]

The long-flagella phenotype in the LF4 variant of *Chlamydomonas reinhardtii*[26] and the elongated photoreceptor cilia reported in the *Mak*-null murine retina[3] prompted the question of whether there would be any detectable changes in the photoreceptor cilia of the RP patients with *MAK* gene mutations. The resolution constraints of even the most current OCT instrumentation led to the decision to compare the length of inner and outer segments (total thickness) in relation to the photoreceptor cell layer thickness at the locus of measurement in RP patients with *MAK* mutations and in a group with RP but without *MAK* mutations ($n = 11$; ages, 20–65 years). A rod-rich retinal area near the rod hot spot of the superior retina[27] and the cone-rich fovea were chosen for analysis. P9 and P16 were the only patients in our cohort of RP with *MAK* mutations

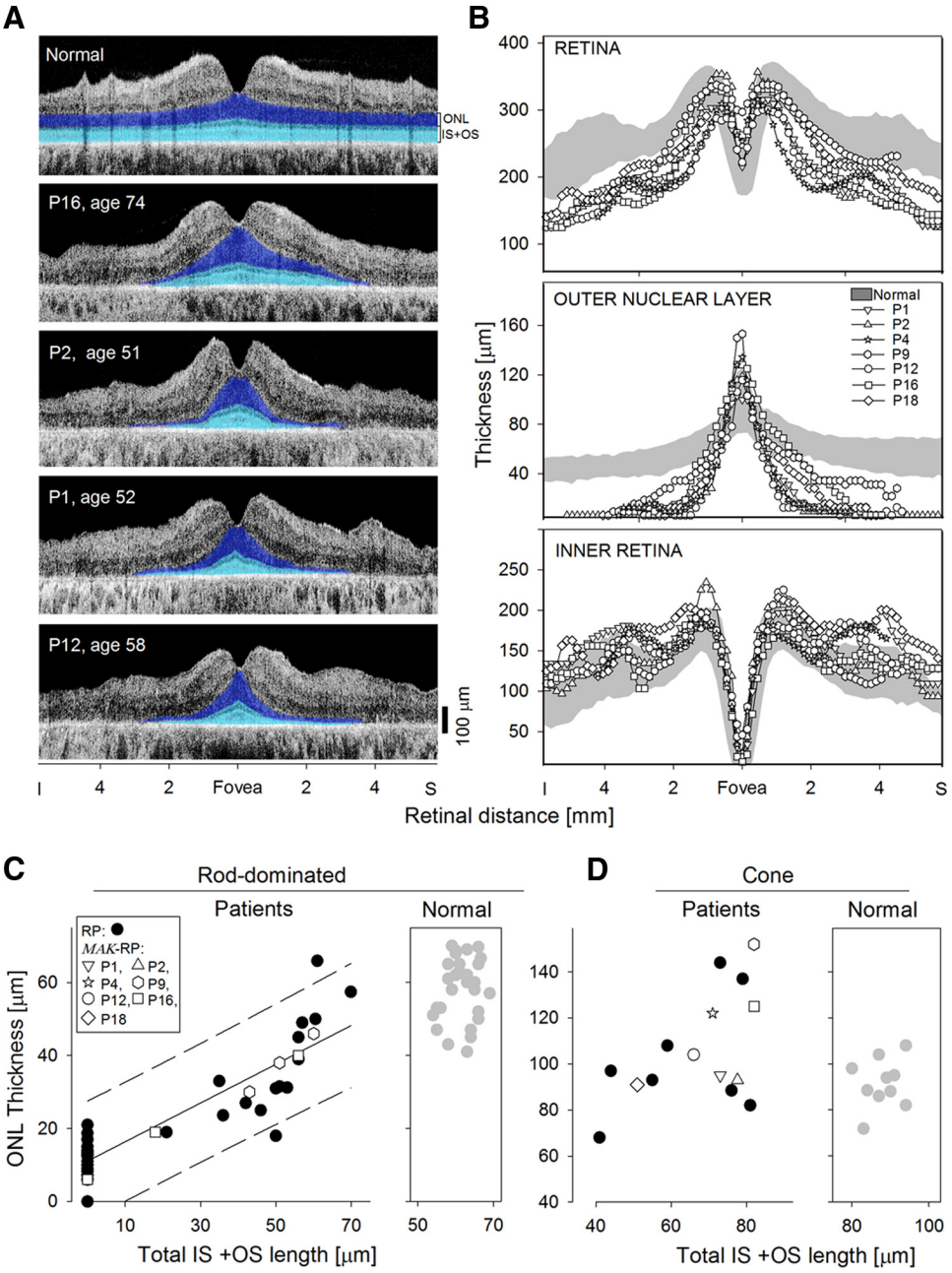

Figure 4. Retinal laminar architecture by OCT in RP with *MAK* mutations. (**A**) SD-OCT scans along the vertical meridian through the fovea in a representative normal subject compared with P16, P2, P1, and P12. Photoreceptor (PR) layers are colorized for visibility: ONL (*dark blue*) and inner and outer segments (*light blue*). (**B**) Thickness of the overall retina (*top*), ONL (*middle*), and inner retina (*bottom*) along the vertical meridian in seven patients with *MAK* mutations. Patients are identified by symbols. *Shaded areas*: normal limits (mean ± 2 SD). (**C**) Inner and outer segments (IS+OS, total thickness) in relation to ONL thickness in a rod-rich region of the superior retina in two RP patients with *MAK* mutations (P9, P16) and in a group with RP without *MAK* mutations (n = 11, ages 20–65; *black circles*). *Solid lines*: the relationship between the parameters; *dashed lines*; 95% confidence limits. *Right inset*: normal data at these superior retinal loci (n = 10; ages 8–45). (**D**) Relationship of IS+OS thickness and ONL thickness at the cone-rich fovea in all seven RP *MAK* patients compared with results in RP patients without *MAK* mutations (n = 8; ages 20–65; three patients excluded because of macular edema or epiretinal membrane distorting foveal architecture).

who had measurable photoreceptor structure in or near the rod hot spot. The relationship of IS+OS to ONL at the loci of measurement in P9 and P16 was no different from that in the RP patients without *MAK* mutations (Fig. 4C). The relationship could be described with linear regression (r^2 = 0.76) and data from P9 and P16 were within the 95% prediction interval defined by the other RP patient data. At the cone-dominated fovea, the thinning of the IS+OS layer was not monotonically related to ONL thickness (Fig. 4D). Thus, a linear regression was not attempted. There appeared to be a tendency for ONL thickening on minor thinning of the IS+OS followed by ONL thinning on further thinning of the IS+OS layer. An exaggerated version of such a reactive retinal thickening has been seen in the foveas of patients with choroideremia.[28]

Discussion

A topography of disease predilection was evident in the patients with *MAK* mutations, and a natural history could be estimated from cross-sectional and longitudinal data. Those with milder disease at the time of first visit showed a gradient of effect from most severe in the superior and temporal visual fields to least severe in the inferior and nasal fields. Disease progression led to nearly complete loss of temporal field function, but a more preserved nasal field. Other patterns indicated that midperipheral scotomas progressed and separated the well-preserved central island from a nasal and inferior field island. More advanced patterns showed only a retained central island that could become further reduced in extent. Funduscopic features in some patients showed pigmentary abnormalities that were less prominent in the superior and temporal retina than in other quadrants, but in more advanced disease, there was involvement of the entire mid- and far-peripheral retina. Full-field ERG patterns were those of RP: Rod dysfunction was always greater than cone dysfunction, and, in more advanced stages there were nondetectable signals. Among eight patients in a recent report of *MAK* mutations other than

the Alu insertion,[2] sectorial RP was the diagnosis in two patients who had temporal visual field scotomas and nasal retinal funduscopic abnormalities, and there was one patient with a diagnosis of RP who had temporal more than nasal scotomas. All these patients had severely abnormal ERGs suggesting that the superotemporal field sector was more prominent than other sites of visual loss, but this was definitely a widespread and not a delimited retinal disease. Overall, the disease topography that we observed in our cohort of patients with *MAK* mutations was also found in other populations with this specific genetic disease.

Has this pattern of visual loss been noted previously in other forms of RP? In a survey of kinetic field patterns among patients with RP,[29] there are two patterns (IIB and IIC) that resemble the fields in patients in the present study. Some of the examples of IIB and IIC are more of the altitudinal variety, but there are also some superotemporal quadrantic defects. Of interest, all 18 RP patients showing patterns IIB and IIC had autosomal dominant (ad) inheritance.[29] Altitudinal forms of adRP caused by class B1 rhodopsin gene mutations have been well described.[30–32] The field loss in the patients with *MAK* mutations, however, most resembles the pattern we described in patients with adRP caused by *RP1* mutations.[33] Contributing to the regional retinal variations of disease in RP could be topographic differences in gene expression,[34–37] even though such information is currently lacking for most molecules of potential relevance. The similarity of disease expression in *RP1* and *MAK* forms of RP is especially intriguing considering the report of colocalization of Mak with RP1 in the ciliary axoneme of murine photoreceptors and in vitro assays that suggest that RP1 is a phosphorylation target of Mak.[3] Further studies will determine whether the experimental results showing that interaction between Mak and RP1 in the photoreceptor cilium help to explain the greater (or lesser) vulnerability to degeneration of certain regions of the human retina in patients with *MAK*- and *RP1*-associated RP.

Are there OCT-detectable structural features of rod and cone OS abnormalities in RP due to *MAK* mutations that could help explain the progressive degeneration of the photoreceptors? Common molecular forms of human RP and their animal models studied to date have shown that loss of photoreceptor nuclei are associated with OS shortening and ONL thinning.[32,38,39] Photoreceptor OS in *Mak*-null mice, on the other hand, show a combination of unusual features including elongated cilia and OS disorganization.[3] Although individual cilia are below the current resolution of OCT methods, we hypothesized that cilial and OS abnormalities in human patients may modify the relationship of the thickness of the inner and outer segment layers with the thickness of the ONL layer. Our quantitative results compared this relationship in the rod-rich region of two arRP *MAK* patients and in the cone-only fovea of 7 arRP *MAK* patients to a group of RP patients without *MAK* mutations; there were no apparent differences. We conclude that either cilial elongation seen in young mice is not a feature of the adult human arRP *MAK* patients, or the effect becomes undetectable with noninvasive methods due to the simultaneous shortening of the OS.

Do we know any more about the natural history of this form of RP as a result of this study and do any of the phenotypic data inform us about strategies for monitoring future clinical trials of therapy? The prolonged survival of the central retinal island with its good acuity (with one exception, P22) seems to be a positive prognostic feature of the *MAK* exon 9 insertion type of arRP. Visual acuity was also well-preserved in at least one eye of the eight patients recently described with other *MAK* mutations (age, 23–67 years).[2] When we quantified the rate of visual field loss, however, it was not correspondingly slow. According to previously reported longitudinal data for RP using the V-4e stimulus, annual exponential rates of field loss have ranged from 4.5% to 13.6% in cohorts of RP patients without molecular diagnoses or with *USH2A* mutations, syndromic and nonsyndromic.[19,21,40–44] The rate of 11% in the present study falls within the range of these other reports. In other words, the rate of field loss does not mirror the time course of acuity loss in arRP *MAK*. There are also implications of our data for the design of outcome measures in future therapeutic trials. Measures of visual acuity would not be a good way to monitor this disease through a trial and foveal targeting of treatment would seem imprudent. Depending on the type of therapeutic approach, rod and/or cone thresholds in the oft-preserved but still vulnerable superotemporal retina seems to be a more telling metric.

The identification of *MAK* adds another gene to the growing list of frequent causes of autosomal recessive retinal degenerations in the Ashkenazi Jewish population. Currently, the relatively common *PCDH15* and *CLRN1* mutations are included on some AJ carrier screening panels, and interest in these tests has been high, despite relatively low carrier frequencies.[18] Carrier screening panels should be further expanded to include the *MAK* gene as an option, with appropriate genetic counseling. The screening strategy in AJ patients with simplex, multiplex, and recessive RP can also be further refined. It seems appropriate to include *MAK* in a first-tier genetic screening of these patients.

References

1. Tucker BA, Scheetz TE, Mullins RF, et al. Exome sequencing and analysis of induced pluripotent stem cells identify the cilia-related gene male germ cell-associated kinase (MAK) as a cause of retinitis pigmentosa. *Proc Natl Acad Sci U S A;*. 2011;108:E569–E576.
2. Ozgul RK, Siemiatkowska AM, Yucel D, et al. Exome Sequencing and cis-regulatory mapping identify mutations in MAK, a gene encoding a regulator of ciliary length, as a cause of retinitis pigmentosa. *Am J Hum Genet*. 2011;89:253–264.
3. Omori Y, Chaya T, Katoh K, et al. Negative regulation of ciliary length by ciliary male germ cell-associated kinase (Mak) is required for retinal photoreceptor survival. *Proc Natl Acad Sci USA*. 2010; 107:22671–22676.
4. Bramall AN, Wright AF, Jacobson SG, McInnes RR. The genomic, biochemical, and cellular responses of the retina in inherited photoreceptor degenerations and prospects for the treatment of these disorders. *Annu Rev Neurosci.* 2010;33:441–472.
5. Wright AF, Chakarova CF, Abd El-Aziz MM, Bhattacharya SS. Photoreceptor degeneration: genetic and mechanistic dissection of a complex trait. *Nat Rev Genet.* 2010;11:273–284.
6. Herrera W, Aleman TS, Cideciyan AV, et al. Retinal disease in Usher syndrome III caused by mutations in the clarin-1 gene. *Invest Ophthalmol Vis Sci.* 2008;49:2651–2660.
7. Ben-Yosef T, Ness SL, Madeo AC, et al. A mutation of PCDH15 among Ashkenazi Jews with the type 1 Usher syndrome. *N Engl J Med.* 2003;348:1664–1670.
8. Zelinger L, Banin E, Obolensky A, et al. A missense mutation in DHDDS, encoding dehydrodolichyl diphosphate synthase, is associated with autosomal-recessive retinitis pigmentosa in Ashkenazi Jews. *Am J Hum Genet.* 2011;88:207–215.
9. Zuchner S, Dallman J, Wen R, et al. Whole-exome sequencing links a variant in DHDDS to retinitis pigmentosa. *Am J Hum Genet.* 2011;88:201–206.
10. Jacobson SG, Yagasaki K, Feuer WJ, Roman AJ. Interocular asymmetry of visual function in heterozygotes of X-linked retinitis pigmentosa. *Exp Eye Res.* 1989;48:679–691.
11. Jacobson SG, Voigt WJ, Parel JM, et al. Automated light- and dark-adapted perimetry for evaluating retinitis pigmentosa. *Ophthalmology.* 1986;93:1604–1611.
12. Roman AJ, Schwartz SB, Aleman TS, et al. Quantifying rod photoreceptor-mediated vision in retinal degenerations: dark-adapted thresholds as outcome measures. *Exp Eye Res.* 2005;80:259–272.

13. Huang Y, Cideciyan AV, Papastergiou GI, et al. Relation of optical coherence tomography to microanatomy in normal and rd chickens. *Invest Ophthalmol Vis Sci.* 1998;39:2405–2416.
14. Jacobson SG, Cideciyan AV, Aleman TS, et al. Crumbs homolog 1 (CRB1) mutations result in a thick human retina with abnormal lamination. *Hum Mol Genet.* 2003;12:1073–1078.
15. Aleman TS, Cideciyan AV, Sumaroka A, et al. Retinal laminar architecture in human retinitis pigmentosa caused by Rhodopsin gene mutations. *Invest Ophthalmol Vis Sci.* 2008;49:1580–1590.
16. Jacobson SG, Aleman TS, Sumaroka A, et al. Disease boundaries in the retina of patients with Usher syndrome caused by MYO7A gene mutations. *Invest Ophthalmol Vis Sci.* 2009;50:1886–1894.
17. Jacobson SG, Cideciyan AV, Aleman TS, et al. Human retinal disease from AIPL1 gene mutations: foveal cone loss with minimal macular photoreceptors and rod function remaining. *Invest Ophthalmol Vis Sci.* 2011;52:70–79.
18. Scott SA, Edelmann L, Liu L, Luo M, Desnick RJ, Kornreich R. Experience with carrier screening and prenatal diagnosis for 16 Ashkenazi Jewish genetic diseases. *Hum Mutat.* 2010;31:1240–1250.
19. Berson EL, Sandberg MA, Rosner B, Birch DG, Hanson AH. Natural course of retinitis pigmentosa over a three-year interval. *Am J Ophthalmol.* 1985;99:240–251.
20. Birch DG, Anderson JL, Fish GE. Yearly rates of rod and cone functional loss in retinitis pigmentosa and cone-rod dystrophy. *Ophthalmology.* 1999;106:258–268.
21. Iannaccone A, Kritchevsky SB, Ciccarelli ML, et al. Kinetics of visual field loss in Usher syndrome type II. *Invest Ophthalmol Vis Sci.* 2004;45:784–792.
22. Cideciyan AV, Swider M, Aleman TS, et al. ABCA4 disease progression and a proposed strategy for gene therapy. *Hum Mol Genet.* 2009;18:931–941.
23. Berson EL, Rosner B, Weigel-DiFranco C, Dryja TP, Sandberg MA. Disease progression in patients with dominant retinitis pigmentosa and rhodopsin mutations. *Invest Ophthalmol Vis Sci.* 2002;43:3027–3036.
24. Oh KT, Longmuir R, Oh DM, et al. Comparison of the clinical expression of retinitis pigmentosa associated with rhodopsin mutations at codon 347 and codon 23. *Am J Ophthalmol.* 2003;136:306–313.
25. Aleman TS, Cideciyan AV, Sumaroka A, et al. Inner retinal abnormalities in X-linked retinitis pigmentosa with RPGR mutations. *Invest Ophthalmol Vis Sci.* 2007;48:4759–4765.
26. Berman SA, Wilson NF, Haas NA, Lefebvre PA. A novel MAP kinase regulates flagellar length in Chlamydomonas. *Curr Biol.* 2003;13:1145–1149.
27. Curcio CA, Sloan KR, Kalina RE, Hendrickson AE. Human photoreceptor topography. *J Comp Neurol.* 1990;292:497–523.
28. Jacobson SG, Cideciyan AV, Sumaroka A, et al. Remodeling of the human retina in choroideremia: rab escort protein 1 (REP-1) mutations. *Invest Ophthalmol Vis Sci.* 2006;47:4113–4120.
29. Grover S, Fishman GA, Brown J Jr. Patterns of visual field progression in patients with retinitis pigmentosa. *Ophthalmology.* 1998;105:1069–1075.
30. Stone EM, Kimura AE, Nichols BE, Khadivi P, Fishman GA, Sheffield VC. Regional distribution of retinal degeneration in patients with the proline to histidine mutation in codon 23 of the rhodopsin gene. *Ophthalmology.* 1991;98:1806–1813.
31. Heckenlively JR, Rodriguez JA, Daiger SP. Autosomal dominant sectoral retinitis pigmentosa: two families with transversion mutation in codon 23 of rhodopsin. *Arch Ophthalmol.* 1991;109:84–91.
32. Cideciyan AV, Hood DC, Huang Y, et al. Disease sequence from mutant rhodopsin allele to rod and cone photoreceptor degeneration in man. *Proc Natl Acad Sci U S A.* 1998;95:7103–7108.
33. Jacobson SG, Cideciyan AV, Iannaccone A, et al. Disease expression of RP1 mutations causing autosomal dominant retinitis pigmentosa. *Invest Ophthalmol Vis Sci.* 2000;41:1898–1908.
34. Sakuta H, Suzuki R, Takahashi H, et al. Ventroptin: a BMP-4 antagonist expressed in a double-gradient pattern in the retina. *Science.* 2001;293:111–115.
35. Sharon D, Blackshaw S, Cepko CL, Dryja TP. Profile of the genes expressed in the human peripheral retina, macula, and retinal pigment epithelium determined through serial analysis of gene expression (SAGE). *Proc Natl Acad Sci USA.* 2002;99:315–320.
36. Cornish EE, Madigan MC, Natoli R, Hales A, Hendrickson AE, Provis JM. Gradients of cone differentiation and FGF expression during development of the foveal depression in macaque retina. *Vis Neurosci.* 2005;22:447–459.
37. Tanito M, Kaidzu S, Ohira A, Anderson RE. Topography of retinal damage in light-exposed albino rats. *Exp Eye Res.* 2008;87:292–295.
38. Milam AH, Li ZY, Fariss RN. Histopathology of the human retina in retinitis pigmentosa. *Prog Retin Eye Res.* 1998;17:175–205.
39. Machida S, Kondo M, Jamison JA, et al. P23H rhodopsin transgenic rat: correlation of retinal function with histopathology. *Invest Ophthalmol Vis Sci.* 2000;41:3200–3209.
40. Massof R, Dagnelie G, Benzschawel T, Palmer R, Finkelstein D. First-order dynamics of visual field loss in retinitis pigmentosa. *Clin Vision Sci.* 1990;5:1–26.
41. Holopigian K, Greenstein V, Seiple W, Carr RE. Rates of change differ among measures of visual function in patients with retinitis pigmentosa. *Ophthalmology.* 1996;103:398–405.
42. Grover S, Fishman GA, Anderson RJ, Alexander KR, Derlacki DJ. Rate of visual field loss in retinitis pigmentosa. *Ophthalmology.* 1997;104:460–465.
43. Fishman GA, Bozbeyoglu S, Massof RW, Kimberling W. Natural course of visual field loss in patients with type 2 Usher syndrome. *Retina.* 2007;27:601–608.
44. Sandberg MA, Rosner B, Weigel-DiFranco C, McGee TL, Dryja TP, Berson EL. Disease course in patients with autosomal recessive retinitis pigmentosa due to the USH2A gene. *Invest Ophthalmol Vis Sci.* 2008;49:5532–5539.